TÜBİTAK

Turkish Journal of Chemistry

http://journals.tubitak.gov.tr/chem/

Research Article

Turk J Chem
(2017) 41: 648 – 657

doi:10.3906/kim-1609-69

Photoemissive polymer composite based on new Y(III), Gd(III), and Tb(III) complexes with N-hydroxyphthalimide

Catalina Yarodara ROSCA, Petronela HORLESCU, Corneliu S. STAN*, Daniel SUTIMAN

Department of Chemical Engineering, Faculty of Chemical Engineering and Environmental Protection, Gheorghe Asachi Technical University of Iasi, Iasi, Romania

Received: 28.09.2016 • **Accepted/Published Online:** 13.03.2017 • **Final Version:** 10.11.2017

Abstract: In the present work, a green emitting composite with attractive photoluminescent properties was obtained through the embedding of the Tb^{3+} complex with N-hydroxyphthalimide in a poly-(N-vinyl-pyrrolidone) matrix, which was further processed in thin or thick films. First, several complexes of Gd^{3+}, Tb^{3+}, and Y^{3+} with N-hydroxyphthalimide with the general formula $[M(NHF)_3(DMF)_2]$ were prepared at a 1:3 metal/ligand ratio. The Tb^{3+} complex presents specific emission peaks, with the most intense peak located at 543 nm, thus being selected for incorporation in the poly(N-vinyl-pyrrolidone) matrix. The prepared complexes and composites were investigated through elemental analysis, thermal analysis, FT-IR, P-XRD, and SEM. The photoluminescent properties were studied in detail. Remarkably, through the embedding in the poly(vinyl-pyrrolidone) matrix, the photoluminescent properties of the Tb^{3+} complex are notably enhanced compared to the free complex.

Key words: Luminescent complexes, poly-(N-vinyl-pyrrolidone), luminescent polymer composites

1. Introduction

During the last decades, growing research interest was noted for developing of new photoluminescent compounds and materials for optoelectronic devices, special purpose inks or coatings, bioimaging assays, etc.[1,2] Many of their applications focused on optoelectronics devices ranging from LEDs and OLEDs[3,4] to solar cells or fiber optics communications.[5,6] The majority of lanthanide luminescent species are complexes with phenanthroline, pyridine, triazoles, hydroxyphthalimide, hydroxy isophthalaldehyde, and 1,3-diketones.[7–10] Well known for their applications in medical imaging, gadolinium and terbium complexes have several advantages such as high contrasting efficiency and relatively low toxicity.[11–15] In a different approach, nanoparticles assembled from terbium and gadolinium 1,3-diketones with applications in biolabeling are obtained through a simple path allowing the preparation of core-shell colloids with impressive magnetofluorescent properties.[16] Materials based on yttrium complexes are attractive due to their potential applications in lasers, optics, displays, sensors, or catalysts and experimental studies led to several materials being deemed useful for applications in electroluminescent devices.[17,18] Regarding polymer composites, polystyrene (PS), polycarbonate (PC), poly-(N-vinyl-pyrrolidone) (PVP), poly-(vinyl alcohol) (PVA), and poly-(methyl methacrylate) (PMMA) were successfully used as matrices for the preparation of photoluminescent composites. In this context, photoluminescent polymer composites

*Correspondence: stcornel@gmail.com

were obtained by introducing graphene complexes or quantum dots in PVA matrices. The obtained materials can be used in light-emitting diodes or flexible electronic displays.[19,20] An interesting approach focused on obtaining active laser mediums. In this sense, Jusza et al. reported investigations over photoemissive PMMA nanocomposites doped with YF_3, YOF, and Y_2O_3 and activated by Pr^{3+} ions, which, through the combination of their advantages such as price and mechanical and optical properties, could be widely used in high-bandwidth telecommunications systems and optical integrated optoelectronics[21]. PVP is especially interesting due to its optical transparency, solubility in DMF, and low cost and also because of the possibility to be cross-linked to obtain composites with improved thermal stability and mechanical strengths.[22] Sivaiah et al. reported the introduction of divalent ions Cu and Co in a PVP matrix, the resulting materials presenting encouraging optical properties[23]. In another approach, PVP-based composite fibers with diameters of 500 nm were obtained through electrospinning, by inserting europium complexes with TTA (thenoyltrifluoroacetone) and TPPO (triphenylphosphine oxide) in the polymer matrix[24]. By introducing Sm^{3+} and Tb^{3+} with salicylic acid and 1,10-phenanthroline complexes in PVA matrices, photoluminescent polymer composites with a combination of blue, green, and red-orange emissions for white lighting devices were obtained.[25]

The present work reports the successful preparation of three new luminescent complexes of Gd^{3+}, Tb^{3+}, and Y^{3+} with N-hydroxyphthalimide as a ligand. The prepared Tb^{3+} complex was selected due to its impressive photoluminescent emission to further prepare a composite using PVP as a polymer matrix. The prepared composite was investigated in detail, several interesting conclusions being drawn afterwards. The PVP–$[Tb(NHF)_3(DMF)_2]$ composite exhibits an intense green emission and very good processability in thin or thick films, being a good candidate for applications in optoelectronics.

2. Results and discussion

2.1. Chemical analysis

Data provided by elemental analysis in the case of the free ligand and prepared complexes are presented in Table 1. The experimental results are in very good agreement with the theoretical values, supporting the 1:3 metal to ligand ratio, and also with the results obtained from thermal analysis. The experimental data are in accordance with the proposed chemical formula for each prepared complex.

Table 1. Chemical analysis experimental results compared with calculated values.

Ligand/ complex	Element								Formula of complexes
	C [%]		H [%]		N [%]		O [%]		
	Pred.	Exp.	Pred.	Exp.	Pred.	Exp.	Pred.	Exp.	
HL	58.84	59.03	3.06	3.01	8.58	8.21	29.42	28.97	$C_8H_5NO_3$
(1)	45.40	44.84	3.65	3.69	8.82	8.81	22.19	23.01	$[Gd(NHF)_3(DMF)_2]$
(2)	45.31	44.56	3.65	3.87	8.81	8.46	22.15	21.53	$[Tb(NHF)_3(DMF)_2]$
(3)	49.69	48.34	4.00	3.90	9.66	8.88	24.29	23.95	$[Y(NHF)_3(DMF)_2]$

2.2. FT-IR analysis

Figure 1a presents the recorded FT-IR spectra for the free ligand, prepared complexes, and polymer composite. Significant modifications could be noted in the case of the prepared complexes as follows: stretching of the carbonyl groups with the displacement of their characteristic wavenumber to the lower regions of the spectra, the initial peak splitting into two distinct peaks as a result of the coordinative bond established by one of

the two carbonyl groups present in the ligand molecule; the appearance of an absorption peak located in the 430–410 cm^{-1} range, which is specific to the covalent bonding established between the lanthanide cation and the oxygen atom from the –OH group. Based on these results, the bidentate character of the ligand (NHF) is highlighted (covalent bonding M-O-N< and coordinative bonding M—O=C<).

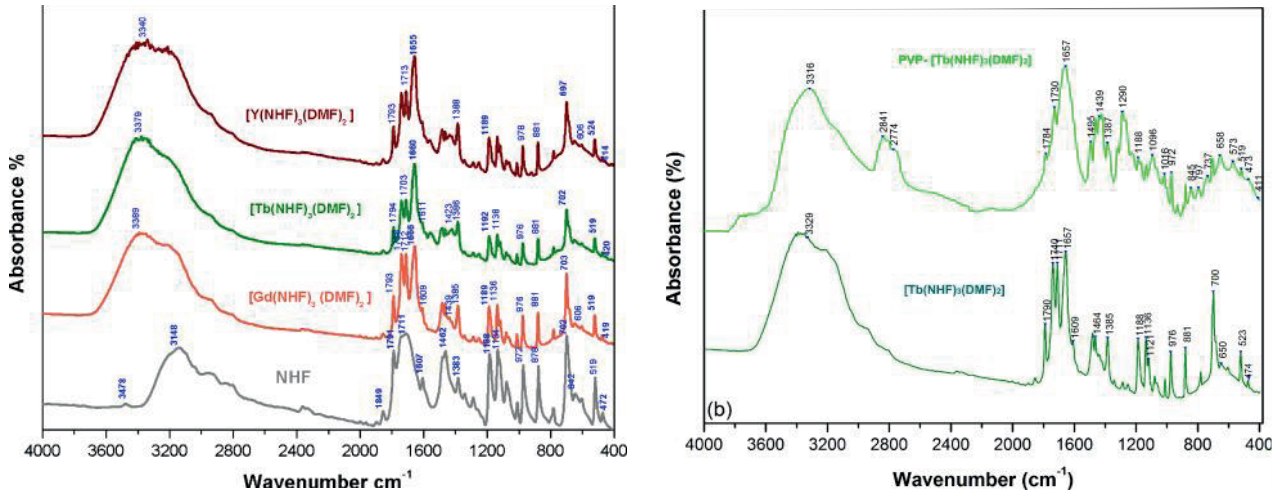

Figure 1. a. FT-IR spectra of the free ligand and $[M(NHF)_3(DMF)_2]$ complexes (M=Y, Tb, Gd). b. FT-IR spectra of the $[Tb(NHF)_3(DMF)_2]$ complex and [PVP- $Tb(NHF)_3(DMF)_2$] composite.

The FT-IR spectrum recorded for the prepared composite (Figure 1b) revealed several modifications compared with the free complex $[Tb(NHF)_3(DMF)_2]$. Due to the ratio between the PVP matrix and the embedded complex, the recorded spectrum is dominated by the characteristic absorption peaks of the polymer matrix, but certain specific peaks of the embedded complexes can be clearly noticed. In addition, the IR spectra sustain interactions between PVP and the metal cation, highlighted by the C=O peak shifting to lower wavenumbers along with a slight asymmetry in the shape of this peak. Several significant peaks recorded for each of the investigated compounds and their assignment are presented in Table 2.

Table 2. Specific vibrations and their assignments to various functional groups recorded for the free ligand, $[Tb(NHF)_3(DMF)_2]$, and [PVP-$Tb(NHF)_3(DMF)_2$] composite.

Functional group/bond	NHF	$[Gd(NHF)_3(DMF)_2]$	$[Tb(NHF)_3(DMF)_2]$	$[Y(NHF)_3(DMF)_2]$	Composite
C-C stretch	1849	1856/1385	1854/1385	1856/1385	1784/1387
C=O sym. stretch		1711	1711	1711	1730
C=O asym. stretch	1711	1657	1657	1657	1657
C= H deformation	1607	1609	1611	1611	1612
N-O stretch	1462	1439/477	1423/474	1437/474	1439
C-H deformation	1383	1385	1386	1385	1387
C-N stretch	1184	1188	1192	1188	1188
N-OH deformation	1134	1136	1138	1136	1016
C-H bend	972	976	976	976	972
C=O deformation	878	881	881	881	845
N-O twisting	642	606	606	606	658
Ln-O	-	419	419	414	411

2.3. Thermal analysis

Based on the recorded derivatograms, the thermal behaviors of the free ligand and prepared complexes were evaluated (Figure 2). Table 3 presents the kinetic parameters calculated with the Freeman–Carroll method. The first stage corresponds to the release of one DMF molecule, which is justified by a value of no more than n $\geq$ 1 (dependence on chemical reaction diffusion) for all complexes. In the second stage, release of DMF molecules continues and decomposition of the complexes starts by release of CO molecules. The weight losses occurring in stages one and two are caused by the removal of two molecules of DMF and six molecules of CO. The third stage corresponds to the release of NO molecule. The upper stages (4 and 5) correspond to the benzene ring oxidation. Taking into account that the solid residue corresponds to the metal oxide, the following mechanism of decomposition is proposed:

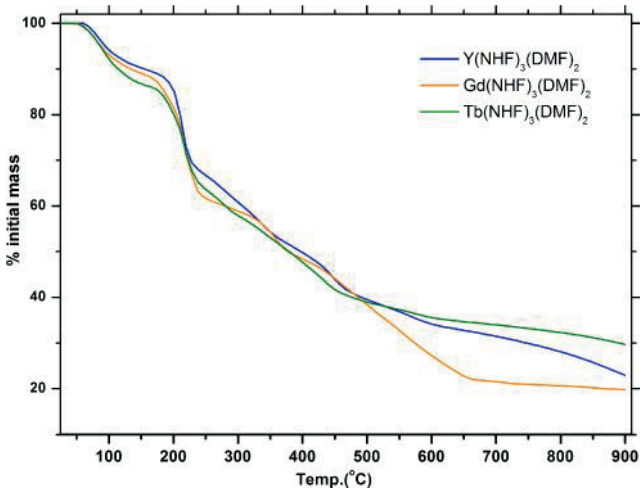

Figure 2. Recorded mass variation of the prepared complexes within the 25–900 °C range.

$$2M[(C_8H_5NO_3)_3(C_3H_7NO)_2] + 42O_2 \rightarrow t\,^{\circ}C \rightarrow M_2O_3 + 4C_3H_7NO + 12CO + 6NO + 36CO_2 + 15H_2O$$

It was also observed that the activation energy is the highest when decomposing the $[Y(NHF)_3(DMF)_2]$ complex, which can be justified by the smallest ionic radius of the Y^{3+} ion compared with the other two cations.

2.4. Powder X-ray diffraction (P-XRD)

Figure 3 presents the recorded diffractograms of the prepared complexes while in Table 4 calculated unit cell parameters are detailed. Throughout the analysis, it was found that the crystallization system is triclinic for Gd^{3+} and Y^{3+} complexes while in the case of the Tb^{3+} complex it is monoclinic. The noticed difference between the crystallization system of the Tb^{3+} complex and Gd^{3+} and Y^{3+} complexes could be explained by the lanthanide contraction,[26] which in the case of the Tb^{3+} complex led to stronger interaction of the cation with the surrounding ligands. Therefore, a more packed configuration occurred in the case of the Tb^{3+} complex, leading to a higher symmetry of the unit cell compared with Gd^{3+} and Y^{3+} complexes.

2.5. Scanning electron microscopy (SEM)

Figure 4 presents the micrographs recorded for a selected complex (Figure 4a) and for the polymer composite (Figure 4b). In the first case, the image highlights the crystalline structure of the complex being in accordance

Table 3. Thermal decomposition stages, reaction order, and activation energies (kJ/mol) of the ligand and prepared complexes.

Decomposition stage	Parameters	$Gd(NHF)_3(DMF)_2$	$Tb(NHF)_3(DMF)_2$	$Y(NHF)_3(DMF)_2$
Stage 1	Ea/kJ mol^{-1}	70.98	71.11	77.00
	N	2.08	1.67	1.89
	Ti	56.63–116.62	68.91–139.41	68.89–123.42
	% loss	12.55	12.00	11.78
Stage 2	Ea/kJ mol^{-1}	94.80	96.31	101.24
	N	0.63	0.55	1.83
	Ti	170.61–234.04	178.83–231.7	184.9–224.49
	% loss	28.09	27.73	31.65
Stage 3	Ea/kJ mol^{-1}	114.69	126.54	146.81
	N	0.46	0.18	0.59
	Ti	322.64–372.62	245.2–292.27	310.29–351.29
	% loss	11.90	12.02	13.06
Stage 4	Ea/kJ mol^{-1}	73.28	77.33	82.08
	n	0.34	0.26	33.1
	Ti	427.35–648.75	320.27–446.75	428.47–457.74
	% loss	10.48	10.91	11.53
Stage 5	Ea/kJ mol^{-1}	68.35	63.59	73.55
	n	0.30	43.5	1.35
	Ti	524.54–648.75	540.3–635.54	520.45–589.54
	% loss	13.7	13.7	16.08
	Residue %*	22.8/23.28	23.04/23.64	15.6/15.9

*Theoretical/experimental E_2O_3.

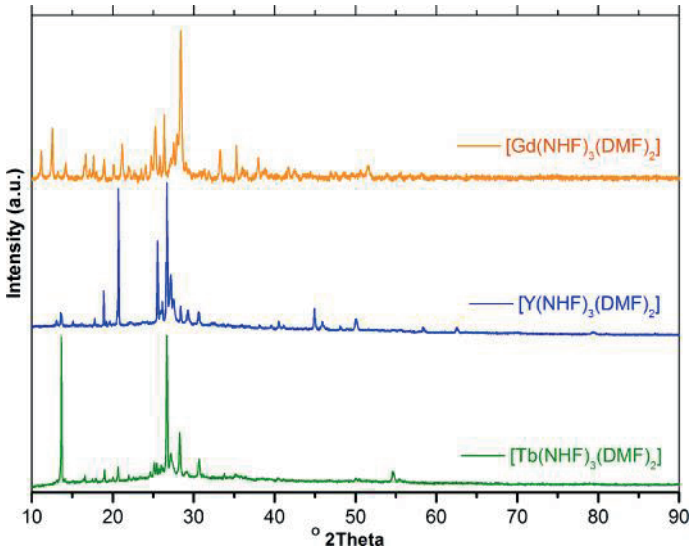

Figure 3. Recorded diffractograms of the prepared complexes.

with the data recorded in the XRD investigation. The average size of the crystallites is in the range of 25–45 μm while an elongated shape is clearly visible. In the case of the prepared composite, the image reveals a relatively uniform presence of the embedded complex within the polymer matrix, with average diameters of the crystallites in the range of 1–5 μm.

Table 4. Calculated unit cell parameters of the ligand and complexes.

HL/complex	a (A°)	b (B°)	c (C°)	α (°)	β (°)	γ (°)	Cell volume, Å^3	Crystallization system
NHF	14.6	9.15	6.88	90	90	90	919.86	Orthorhombic
[Gd(NHF)$_3$(DMF)$_2$]	10.97	13.40	13.06	36.80	126.07	122.41	921.88	Triclinic
[Tb(NHF)$_3$(DMF)$_2$]	19.49	5.78	7.94	90.00	91.30	90.00	895.46	Monoclinic
[Y(NHF)$_3$(DMF)$_2$]	8.44	8.37	13.20	99.63	93.72	105.84	879.35	Triclinic

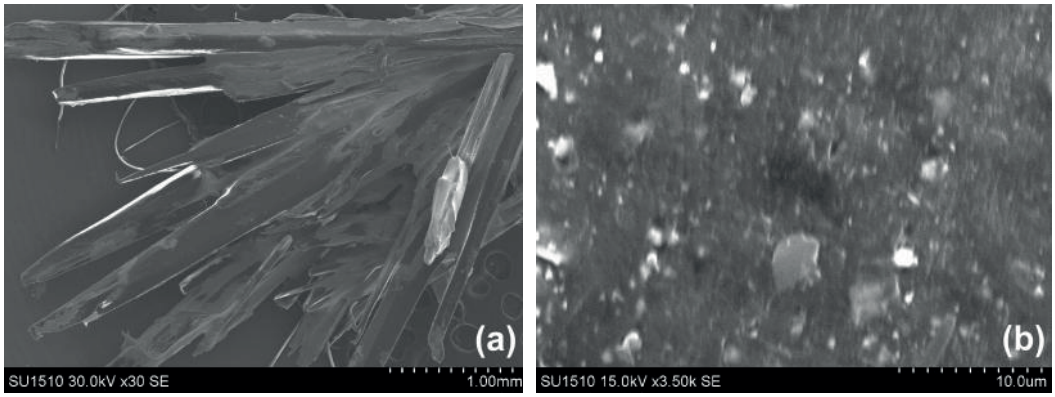

Figure 4. SEM micrographs recorded for (a) [Gd(NHF)$_3$(DMF)$_2$] complex and (b) polymeric composite [PVP-Tb(NHF)$_3$(DMF)$_2$].

2.6. Fluorescence analysis

Figure 5a presents the excitation/emission spectrums recorded for the [Gd(NHF)$_3$(DMF)$_2$] complex. The broadband emission spectrum is centered on a peak located at 500 nm, most probably due to radiative transitions occurring through the influence of the central cation over the excited states of the surrounding ligands.[27] The excitation spectrum revealed also a broader band peak located in the UV-A region at 380 nm. Figure 5b presents the excitation/emission spectra of the yttrium complex. As could be observed, the emission spectrum has a broadband configuration with the peak located at 515 nm. The excitation spectrum has a maximum centered at 437 nm. In the case of the [Y(NHF)$_3$(DMF)$_2$] complex, the wide band emission is governed by the same mechanism involved in the influence of the heavy atom vicinity over the excited states of the ligands. In the case of the [Tb(NHF)$_3$(DMF)$_2$] complex (Figure 5c), the radiative processes rely on the sensitization of the central Tb^{3+} cation through the "antenna effect"[28] induced by the surrounding ligands, which triggers the characteristic narrow emission bands arising from inner transitions within 4f orbitals. The highest intensity emission peak is recorded at 543 nm due to $^5D_4 \rightarrow ^7F_5$ while the second significant peak located at 488 nm is due to the $^5D_4 \rightarrow ^7F_6$ transition. The transition $^5D_4 \rightarrow {}^7F_4$ is responsible for the less intense peak located at 581 nm, while the lowest recorded peak located at 618 nm is due to the $^5D_4 \rightarrow ^7F_3$ transition. The recorded excitation peak is also located in the UV-A region at 377 nm. For comparison, in Figure 5c the excitation and emission spectra of the ligand are also presented. As could be noted, the free ligand presents negligible emission, having two broad emission peaks located at 429 and 463 nm. For the polymer composite PVP–[Tb(NHF)$_3$(DMF)$_2$], the photoluminescence properties were investigated in similar conditions, revealing that the embedded [Tb(NHF)$_3$(DMF)$_2$] complex retains the photoluminescence properties with certain small differences as a result of the reconfigurations induced by the presence of the surrounding polymer matrix. In Figure 5d the excitation/emission spectra recorded for the PVP–[Tb(NHF)$_3$(DMF)$_2$] composite are presented.

No significant differences were noted except for the slight configuration change of the excitation spectrum where distinct peaks located at 351, 358, 368, and 376 nm were recorded.

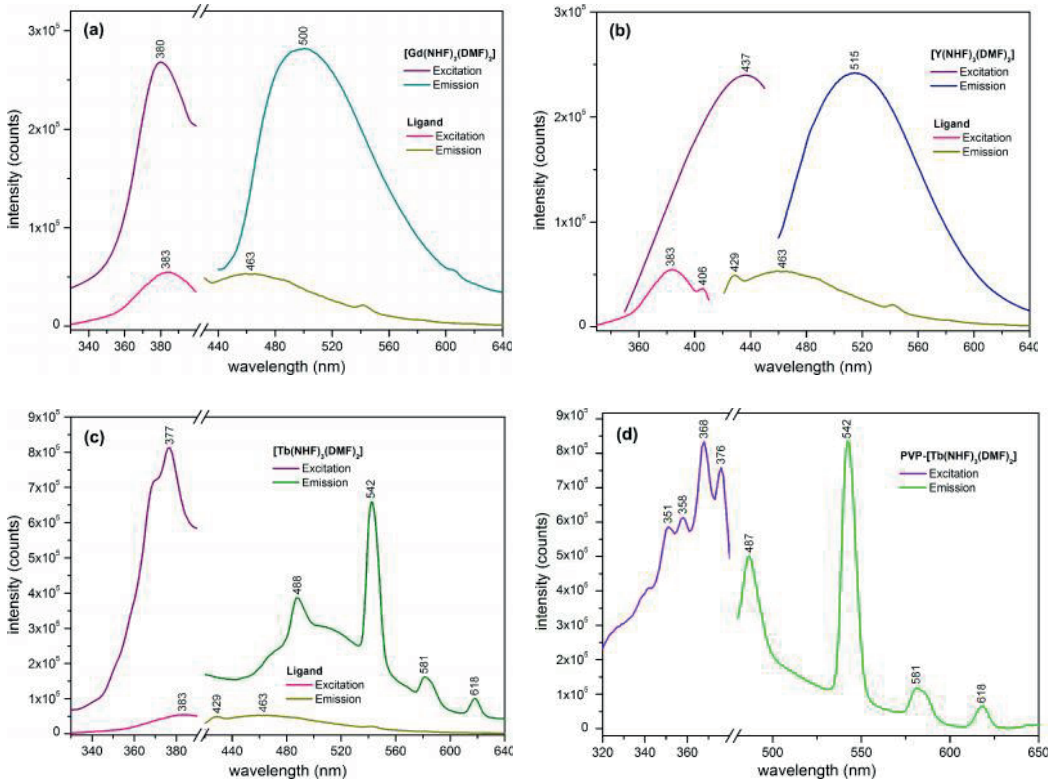

Figure 5. Excitation/emission spectra of prepared (a) Gd^{3+}, (b) Y^{3+}, and (c) Tb^{3+} complexes and (d) PVP–$[Tb(NHF)_3(DMF)_2]$ composite.

As previously mentioned, by embedding the Tb^{3+} complex in the PVP matrix, the PL emission intensity is markedly enhanced. The higher emission intensity is noticeable in terms of visual perception and also is clearly sustained by the absolute PL quantum yield (PLQY) investigation, which revealed markedly improved recorded values in the case of the prepared PVP–$[Tb(NHF)_3(DMF)_2]$ composite. Table 5 presents the recorded values of PLQY at several excitation wavelengths. The highest PLQY value (33.77%) is achieved at an excitation wavelength of 370 nm, while in the case of the free complex the maximum value (19.04%) is recorded at 380 nm.

Table 5. Absolute PLQY values recorded for the prepared Tb^{3+} complex and prepared composite.

λ excitation (nm)	Absolute PLQY (%)	
	$[Tb(NHF)_3(DMF)_2]$	PVP–$[Tb(NHF)_3(DMF)_2]$
360	13.21	24.09
370	16.5	33.77
380	19,04	27.6

The enhancement of the PLQY values through embedding of a photoluminescent complex in polymer matrices was also reported in other studies,[29,30] being most probably a result of the more favorable conditions in terms of excitation energy transfer to the emissive Tb^{3+} centers achieved in the new environment and by the

interactions that occurred between the carbonyl groups in the PVP matrix and the central cation, as highlighted by the FT-IR investigation.

2.7. Conclusions

Three new complexes of Gd^{3+}, Tb^{3+}, and Y^{3+} with N-hydroxyphthalimide were prepared and investigated. This paper also reports a green emitting composite with remarkable photoluminescent properties obtained through embedding of the Tb^{3+} complex with N-hydroxyphthalimide in a poly-(vinyl-pyrrolidone) matrix. Remarkably, through the embedding in the poly-(vinyl-pyrrolidone), the photoluminescent properties are considerably enhanced compared to those of the free complex. The prepared composite was investigated through FT-IR, SEM, and fluorescence spectroscopy. The remarkable photoluminescence of the prepared polymer composite is interesting for potential applications in optoelectronics.

3. Experimental

3.1. Materials

N-Hydroxyphthalimide (97%), poly-(vinyl-pyrrolidone) (molecular weight = 50,000) and N,N-dimethylformamide (99.8%) were purchased from Sigma-Aldrich. Terbium chloride ($TbCl_3 \cdot 6H_2O$, 99.9%), gadolinium chloride ($GdCl_3 \cdot 6H_2O$, 99.9%), and yttrium chloride ($YCl_3 \cdot 6H_2O$, 99.9%) were purchased from Alfa-Aesar.

3.2. Preparation of N-hydroxyphthalimide complexes

All the investigated complexes were prepared at a 1:3 molar ratio (central atom to ligand), the complexation reaction being presented in Figure 6a. First, solutions of gadolinium chloride, terbium chloride, yttrium chloride, and N-hydroxyphthalimide were prepared with concentrations corresponding to 1/3 metal/ligand by dissolving 1 mmol of each of $GdCl_3$, $TbCl_3$, and YCl_3 in 3 mL of N,N-dimethylformamide, while three identical ligand solutions were prepared by dissolving 3 mmol N-hydroxyphthalimide (NHF) in 2 mL of the same solvent. The complexation reactions occurred under moderate stirring at 50–55 °C for about 160 min, the resulting complexes having the molecular formula $[M(NHF)_3(DMF)_2]$. After the evaporation in ambient conditions of the excess solvent, the complexes were obtained in a yellow solid crystallized form. They were then further dried in an oven at 60 °C under vacuum to constant weight. In the second step, the PVP polymer (molecular weight: 50,000) was dissolved by vigorous stirring at 50–55 °C in the same solvent (DMF), thus obtaining a viscous polymer solution. The third stage involved the mixture by vigorous stirring of the $[Tb(NHF)_3(DMF)_2]$ complex solution with the polymer solution. The resulting composite solution was processed by spin or spray coating for the production of thin layers (Figure 6b) or transferred into molds (containers) having the desired geometry to obtain thicker films (Figure 6c).

3.3. Characterization

Elemental chemical analysis was performed on Thermo Fisher Scientific Flash EA-1112 CHNS/O equipment provided with Eager 300 software. The IR spectrum was recorded in the 4000–400 cm^{-1} range using a Digilab FTS-2000 FT-IR spectrometer according to the KBr pellet method. The thermal stability was studied on a Mettler Toledo TGA-SDTA851e under an air flow rate of 20 mL/min. The heating rate was adjusted to 10 °C/min in the range of 50–900 °C. XRD patterns were recorded in the 5–70° 2θ range on a PANalytical X'Pert Pro diffractometer provided with a Cu Kα radiation source (k = 0.154060 nm). Unit cell parameters of the

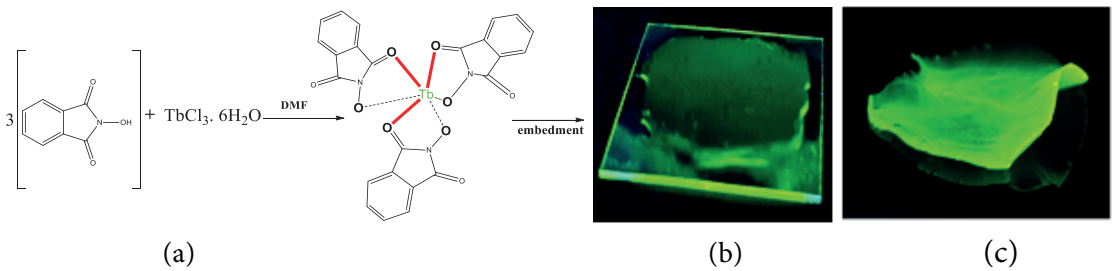

Figure 6. (a) Reaction path and structure of the prepared complexes; (b) thin composite film spin coated on glass; (c) thick composite film of [PVP-Tb(NHF)$_3$(DMF)$_2$].

investigated complexes were further refined with the help of PANalytical X'Pert High Score Plus software. SEM micrographs were obtained by means of Hitachi SU-1510 equipment operated at 10–30 kV accelerating voltage. The steady-state fluorescence and absolute quantum yields (PLQY) were recorded on a Horiba Fluoromax 4P provided with the Quanta-Φ integration sphere. Visual testing of photoluminescent properties was performed using a Philips UVA TL4WBLB lamp with the emission maximum located in the 370–390 nm range.

Acknowledgment

This work was supported by a grant of the Romanian National Authority for Scientific Research (CNCS – UEFISCDI, Project Number PN-II-ID-PCE 2011-3-0708-PN-II IDEI 335/2011).

References

1. Vuojola, J. *Luminescent lanthanide Reporters: New Concepts for Use in Bioanalytical Applications*; Painosalama Oy: Turku, Finland, 2013.
2. Humphreys, M. F. *The Use of Polymer Composites in Construction*; SASBE: Sydney, Australia, 2003.
3. Meng, G.; Chen, Z.; Tang, H.; Liu, Y.; Wei, L.; Wang, Z. *New J. Chem.* **2015**, *39*, 9535-9542.
4. Escudero, D.; Jacquemin, D. *Dalton Trans.* **2015**, *44*, 8346-8355.
5. Bünzli, J. C. G.; Piguet, C. *Chem. Soc. Rev.* **2005**, *34*, 1048-1077.
6. Eliseeva, S. V.; Bünzli, J. C. G. *Chem. Soc. Rev.* **2010**, *39*, 189-227.
7. Tao, C.; Du, K.; Yin, Q.; Zhu, J.; Yan, H.; Zhu, F.; Zhang, L. *RSC Adv.* **2015**, *5*, 58936-58942.
8. Stan, C. S.; Peptu, C.; Marcotte, N.; Horlescu, P.; Sutiman, D. *Inorg. Chim. Acta* **2015**, *429*, 160-167.
9. Lin, P. H.; Leclère, M.; Long, J.; Burchell, T. J.; Korobkov, I.; Clérac, R.; Murugesu, M. *Dalton Trans.* **2010**, *39*, 5698-5704.
10. Binnemans, K. In: *Handbook on the Physics and Chemistry of Rare Earths*; Gschneidner K. A., Ed. Elsevier: Amsterdam, the Netherlands, 2005, pp. 107-272.
11. Yang, C. T.; Chuang, K. H. *Med. Chem. Commun.* **2012**, *3*, 552-565.
12. Hermann, P.; Kotek, J.; Kubíček, V.; Lukeš, I. *Dalton Trans.* **2008**, *23*, 3027-3047.
13. Zhou, Z.; Lu, Z. R. *Wiley Interdiscip. Rev. Nanomed. Nanobiotechnol.* **2013**, *5*, 1-18.
14. Stan, C. S; Sibiescu, D.; Cretescu, I.; Rosca, C. Y.; Sutiman, D.; Tutulea, D. M.; Rosca, I. *Optoelectron. Adv. Mat.* **2011**, *5*, 994-998.
15. Shamsutdinova, N. A.; Podyachev, S. N.; Sudakova, S. N.; Mustafina, A. R.; Zairov, R. R.; Burilov, V. A.; Nizameev, I. R.; Rizvanov, I. K.; Syakaev, V. V.; Gabidullin, B. M. et al. *New J. Chem.* **2014**, *38*, 4130-4140.
16. Zairov, R.; Mustafina, A.; Shamsutdinova, N. *Nature Scientific Reports* **2017**, *7*, 40486.

17. Bortoluzzi, M.; Bianchin, E.; Roppa, S.; Bertolasi, V.; Enrichi, F. *Dalton Trans.* **2014**, *43*, 10120-10131.

18. Abdelrazek, E. M.; Ragab, H. M.; Abdelaziz, M. *Plastic and Polymer Technology* **2013**, *2*, 1-8.

19. Kovalchuk, A.; Huang, K.; Xiang, C.; Martí, A. A.; Tour, J. M. *ACS Appl. Mater. Interfaces* **2015**, *7*, 26063-26068.

20. Liang, R.; Yan, D.; Tian, R., Yu, X.; Shi, W.; Li, C.; Wei, M.; Evans, D. G.; Duan, X. *Chem. Mater.* **2014**, *26*, 2595-2600.

21. Jusza, A.; Lipinska, L.; Polis P.; Piramidowicz, R. In: *Lasers and Electro-Optics Europe* (CLEO EUROPE/IQEC) *Conference on International Quantum Electronics*, 2013.

22. Shahroosvand, H.; Najafi, L.; Mohajerani, E.; Khabbazi, A.; Nasrollahzadeh, M. *J. Mater. Chem. C* **2013**, *1*, 1337-1344.

23. Sivaiah, K.; Rudramadevi, B.; Hemalatha Buddhudu, S. *Indian J. Pure Ap. Phy.* **2010**, *48*, 658-662.

24. Zhang, H.; Song, H.; Yu, H.; Li, S.; Bai, X.; Pan, G.; Dai, Q.; Wang, T.; Li, W.; Lu, S. et al. *Appl. Phys. Lett.* **2007**, *90*, 103103.

25. Kaur, G.; Rai, S. B. *J. Phys. D Appl. Phys.* **2011**, *44*, 425306.

26. Sairenji, S.; Akine, S.; Nabeshima, T.; *Dalton Trans.* **2016**, *45*, 14902-14906.

27. Vogler, A.; Kunkely, H. *Inorg. Chim. Acta* **2006**, *359*, 4130.

28. Zairov, R.; Shamsutdinova, N.; Podyachev, S.; Sudakova S.; Gimazetdinova, G.; Rizvanov, I.; Syakaev, V.; Babaev, V.; Amirov, R.; Mustafina, A. *Tetrahedron* **2016**, *72*, 2447-2455.

29. Li, T.; Shang, W.; Zhang, F.; Mao, L.; Tang C.; Song, M.; Du, C.; Wu, Y. *Engineering* **2011**, *3*, 301-311.

30. Stan, C. S.; Horlescu, P.; Popa, M.; Coroaba, A.; Ursu, L. *New. J. Chem.* **2016**, *40*, 6505-6512.